Journal Pre-proofs

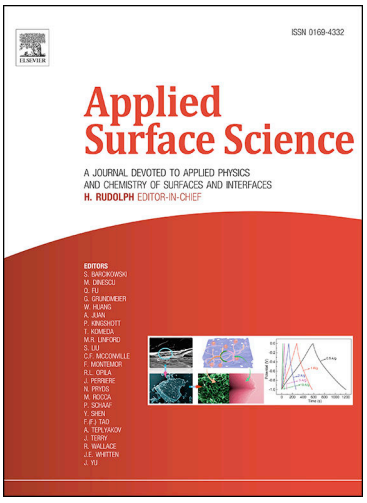

Full Length Article

Emergence of near-zero temperature coefficient of resistance in the Mn_3CuN antiperovskite thin film structure

Cecil Cherian Lukose, Guillaume Zoppi, Martin Birkett

PII: S0169-4332(25)00060-1
DOI: https://doi.org/10.1016/j.apsusc.2025.162347
Reference: APSUSC 162347

To appear in: *Applied Surface Science*

Received Date: 3 November 2024
Revised Date: 20 December 2024
Accepted Date: 8 January 2025

Please cite this article as: C. Cherian Lukose, G. Zoppi, M. Birkett, Emergence of near-zero temperature coefficient of resistance in the Mn_3CuN antiperovskite thin film structure, *Applied Surface Science* (2025), doi: https://doi.org/10.1016/j.apsusc.2025.162347

Emergence of near-zero temperature coefficient of resistance in the Mn_3CuN antiperovskite thin film structure

Cecil Cherian Lukose, Guillaume Zoppi, Martin Birkett*

Faculty of Engineering and Environment, Northumbria University, Newcastle upon Tyne, NE1 8ST, UK.

* Corresponding Author: martin.birkett@northumbria.ac.uk

Abstract

Thin film material systems with extremely low temperature coefficient of resistance (TCR) are highly sought for the fabrication of high precision electronic devices to replace existing nichrome and tantalum nitride technologies. Using reactive magnetron sputtering in a mixed argon/nitrogen atmosphere we produced Mn_3CuN antiperovskite thin film structures and by careful control of the deposition parameters, reveal the emergence of near-zero TCR values. Optimum properties were obtained for films deposited at 0.2-0.3 Pa in a 17% partial nitrogen plasma environment and following heat treatment (nitrogen at 325°C) and stabilisation (air at 260°C), with average TCR values reaching -6 ppm/°C and resistance stability as low as 0.57% for unprotected films. We present full compositional, morphological and structural characterisation of the films and demonstrate that dense and stable Mn_3CuN antiperovskite structures can be successfully grown by reactive magnetron sputtering for the future development of high precision thin film resistive components.

Keywords

Sputter deposition; thin film; antiperovskite; heat treatment; temperature coefficient of resistance.

1. Introduction

Thin film resistive material systems with extremely low temperature coefficient of resistance (TCR) values and electrical resistance stability are sought after for the fabrication of resistive components in electronic systems like global positioning systems (GPS), temperature and flow control sensors for automobile applications and high precision measurement in medical diagnostics, military and aerospace applications [1-7]. Nichrome (NiCr), tantalum nitride (TaN) and ruthenium based oxides are industry favourites in these applications but are now reaching their performance limits [8]. Antiperovskite manganese compounds (Mn_3AN, where A = Cu, Ag, Zn etc.) are emerging as a viable alternative to NiCr because of their unique properties like giant magnetoresistance, negative thermal expansion, magnetocaloric effects, magnetostriction and extremely low TCR values [1, 4, 9-17]. These unique properties are a result of changes in the electronic and magnetic transport properties of the structure resulting from the introduction of various transition metals at the lattice corner sites [18]. Strong hybridization between 2p orbitals of N and 3d orbitals of Mn, creates a tightly bound octahedron unit of 6 Mn atoms bonded with the N atom in the centre of the cell [1, 4, 19, 20]. This facilitates the introduction of 8 other transition metal atoms at the cubic corners, which are weakly bound to the N atom in the centre.

The effect of introducing Cu into the Mn_3AN antiperovskite to form the bulk Mn_3CuN material system was first studied by Chi *et al*. in 2001, and they suggested this particular composition as a suitable candidate to challenge the long established resistive material systems like NiCr due to its high electrical resistivity, very low TCR of 46 ppm/°C and good stability in air [6]. Takenaka *et al*. (2011, 2013) and Ding *et al*. (2011) achieved even lower TCR values in bulk structures of Mn_3AgN and Mn_3NiN by doping Cu at the loosely bound corner sites [5, 21, 22]. Ding *et al*. were able to achieve a stable and reproducible TCR value of 22 ppm/°C for the $Mn_3Ni_{0.7}Cu_{0.3}N$ composition [5], while Takenaka *et al*. (2011) reported TCR values as low as 6 ppm/°C for their study on $Mn_3Ag_{1-X}Cu_XN$ (X=0.32), making these materials potentially more suitable for low TCR applications than commercially available materials like manganin [21]. In their further work, Takenaka *et al*. (2013) were able to achieve an even better TCR value of 0.42 ppm/°C and a resistance drift rate of only 9.1 μΩ/Ω/year [22]. However, very few studies have been conducted to relate the effect of partially doping the corner sites with transition metal atoms to the extremely low TCR nature of these Mn based antiperovskite structures.

These unique properties of antiperovskites are known to be sensitive to dimensional effects, stoichiometry, microstructure, and crystallinity, which are all affected by the method of fabrication. Antiperovskite materials are generally prepared by a solid state sintering technique, in which a weighed amount of Mn is fired along with other doping elements in a nitrogen environment at very high temperature of the order of 700-800°C in a sealed vacuum environment [1]. However, this method of growing bulk material is very challenging as the high temperature environment leads to dissociation of nitrogen [23] and the sintering process has to be performed repeatedly in order to achieve a single phase crystal structure [1, 4]. Antiperovskite fabrication through sintering processes is also not reliable and/or repeatable for large-scale, high-volume manufacturing. While the low TCR nature of Mn based antiperovskites in bulk form have been studied extensively, very few efforts have been made to study this unique property in their thin film format [3, 12, 18].

The relatively high cost of such precision electronic devices is driven partially by the use of costly rare metals such as ruthenium and tantalum in their construction and also because only a small percentage of components produced have the required near zero TCR value, and the rest are rejected [5]. This challenge presents an opportunity for the development of a low cost, high precision thin film Mn based antiperovskite material, made without any rare earth metals and having extremely low TCR. One suitable method to fabricate this type of material is reactive sputtering, which is a well-developed and low cost process for the deposition of oxide and nitride films, and can be easily upscaled from a small laboratory experiment to a full scale industrial production facility [18].

This work demonstrates the first attempt to fabricate the Mn_3CuN antiperovskite structure in thin film form by reactive co-sputtering in nitrogen environment under varying deposition pressure to harness and fine tune its unique electrical properties like ultra-low TCR and resistance stability close to the ideal values required for fabrication of ultra-precise thin film resistive components.

2. Experimental

2.1 Thin film preparation

A schematic of the thin film preparation process is shown in Figure 1. The Mn_3CuN thin film specimens were deposited by reactive co-sputtering of Mn and Cu in a partial nitrogen (N_2) environment at varying deposition pressures. The sputtering was carried out in a Teer Coatings UDP 350 system loaded with a circular Mn target of 100 mm diameter and 99.95% purity and a rectangular Cu target of dimensions 248 mm x 133 mm and 99.99% purity, both supplied by Testbourne Ltd UK. Pre-cleaned soda lime glass slides (75 mm x 25 mm x 1 mm) and 96% alumina plates (101.6 mm x 101.6 mm x 1 mm) were used as substrates. The alumina plates were pre-scribed [13] in 9 columns by 15 rows to yield 135 individual chips (10.16 mm x 6.35 mm) which were pre-deposited with two Ag conductor pads to form electrical contact with the Mn_3CuN thin films. Prior to deposition, a thin strip of Kapton™ tape was applied to the surface of the glass slides to create a step for film thickness measurement.

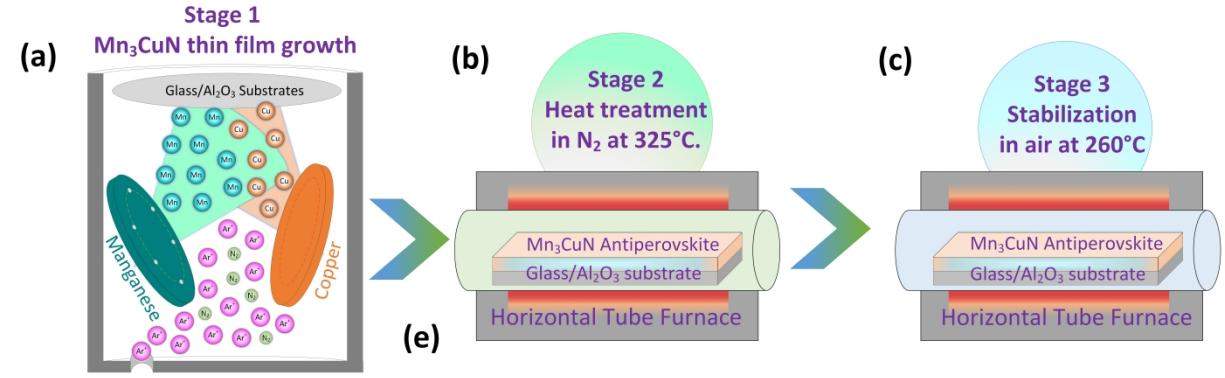

(d)

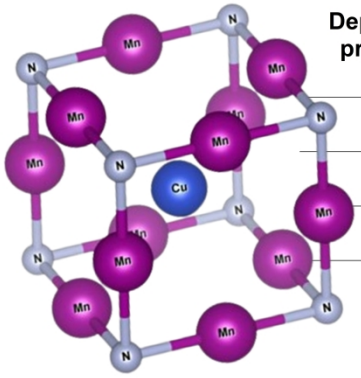

(e)

Deposition pressure (Pa)	Ar flow (sccm)	N_2 flow (sccm)	Total gas flow (sccm)	Partial N_2 (%)	Mn:Cu:N composition (at.%)	Film thickness (nm)
0.2	20	4	24	16.6	59:20:21	460
0.3	25	5	30	16.6	58:20:22	437
0.5	45	7	52	14.0	61:20:19	498

***Figure 1**: Schematic of the Mn_3CuN thin film preparation process. (a) Reactive co-sputtering of Mn and Cu in partial N_2 environment at varying deposition pressures to grow Mn_3CuN thin films, (b) Heat treatment of Mn_3CuN thin films at 325°C in a N_2 environment, (c) heat treatment stabilization in an open-air environment at 260°C for 16 hours, (d) Unit cell projection of stoichiometric Mn_3CuN antiperovskite structure showing local coordination environment of Mn atoms forming stable octahedron (drawn with VESTA visualisation software), and (e) Deposition conditions, chemical composition and thickness of as-grown Mn_3CuN films.*

The thin film samples were grown under controlled room temperature (between 20-25°C). During the deposition, constant DC powers of 300 W and 28 W were applied to the Mn and Cu targets, respectively, to achieve the required chemical composition ratio of 3:1 Mn:Cu in the growing film. Each deposition run was carried out for 90 minutes at a constant rotation speed of 5 rpm and target to substrate distance of 130 mm. The partial N_2 concentration in the Ar:N_2 mixture required to form the Mn_3CuN antiperovskite structure was determined as approximately 14-17% from multiple trial runs for three deposition pressures of 0.2, 0.3 and 0.5 Pa. The upper deposition pressure value of 0.5 Pa was set to be one value higher than our previous work on Mn-based antiperovskites [13], while the lower value of 0.2 Pa was the minimum pressure at which a stable sputtering plasma could be maintained. Following deposition, the as-grown thin films were subjected to heat treatment in a Carbolite TZF 12/75/700e tube furnace at 325°C in a N_2 environment at a constant N_2 flow rate of 2 l/min for 3 hours to stabilize their TCR. A third stage of heat treatment stabilization was then performed on the thin films in an open-air environment at 260°C for 16 hours to improve their electrical resistance stability.

2.2 Thin film characterization

Electrical, structural and morphological studies were performed on as-grown and heat-treated thin films to understand the effect of deposition pressure and heat treatment environment. Four-wire Kelvin sheet resistance measurements were performed at room temperature on the films on alumina substrates using an Agilent 3458A digital multimeter. To measure TCR values, the films were submerged in mineral oil in a Grant LTC1 oil bath and the temperature of the oil was changed between 20 and 70°C using a GD120 thermostat, while the resistance was measured at 20 and 70°C

using the 3458A meter, after allowing it to stabilize for 10 minutes at each end point temperature. TCR was then calculated using the following equation [24]:

$$TCR = \frac{1}{R_{Tref}} \frac{\Delta R}{\Delta T} \times 10^6 \; ppm/°C \qquad (1)$$

Where R_{Tref} is the measured resistance value at 20 °C and ΔR is the change in measured resistance with change in temperature ΔT from 20 to 70 °C. The films resistance stability was measured after the stabilization heat treatment stage by performing a dry heat stability test for 168 hours at 155°C in an open-air environment without any additional layer of protection, and their resistance values were measured every 24 hours (at 155°C) using the 3458A meter. The average, minimum and maximum (error bars) values of sheet resistance, TCR and resistance stability are reported for five thin film resistors selected from the centre and four corners of each pre-scribed alumina plate. Film thicknesses were measured with a Dektak XT stylus profilometer with a 12.5 µm tip by scanning over the step pattern created in the film by Kapton™ tape on the glass substrate. A Tescan MIRA 3 scanning electron microscope (SEM) combined with Oxford Instruments X-Max 150 energy-dispersive X-ray (EDX) detector was used to perform sample imaging and elemental composition analysis. A Siemens X-ray Diffractometer D5000 system employing a Cu *Kα* radiation of wavelength, λ = 1.5418 Å was used to study the crystallinity and structural characteristics of the films. The X-ray diffraction (XRD) measurements were taken over a 2θ range of 20° to 90° in steps of 0.02°. The patterns were analysed using Origin 8.1 and Fityk data processing and nonlinear curve fitting software. Variation in mean crystallite size in the films was calculated from the full-width at half-maximum (FWHM) of the (200) peak of Mn_3CuN using Scherrer's equation [25]. Atomic force microscopy (AFM) was performed using a Veeco Dimension™ 3100 AFM in contact mode over a 3 µm x 3 µm area and used to measure the average roughness (R_a) of the films by mapping the topology of the film surfaces and resolving the measurement data using Gwyddion software [26]. A minimum of 10 samples were characterised for electrical tests and 5 samples or measurement sites for structural and morphological studies, and results for average and range or standard deviation values are presented in the following sections.

3. Results and discussion

Values of Ar and N_2 gas flow rates, chemical composition and average film thickness of Mn_3CuN films grown at the three deposition pressures of 0.2, 0.3 and 0.5 Pa are shown in Figure 1(e). The average chemical composition of Mn:Cu:N remained close to the required 60:20:20 at. % ratio (within the accuracy of EDX) and within ±0.3 at. % for all three deposition pressures. The level of N in the films was seen to vary slightly from 19 to 21 at. % with change in pressure, which could be attributed to adjustments in gas flows made to achieve the required varying working pressures. It was also noticed that the composition of Mn varies from 59 to 61 at. %, directly in relation to N in the film, which is expected because of the strong octahedron bond formed between Mn and N atoms. Throughout the pressure range, it was observed that the level of Cu in the films remains constant at 20 at.%. The effect of working pressure on film thickness is not very clear in the literature as there are contradictory claims about increasing film thickness with increasing working pressure [27] and vice versa [28]. However, in this work the thickness of the Mn_3CuN films seems relatively unaffected

by working pressure and all samples are within ± 10%. The lowest thickness of 437 nm is achieved for films grown at 0.3 Pa, followed by films deposited at 0.2 Pa (460 nm) and then films deposited at 0.5 Pa at 498 nm. Overall, both chemical composition and film thickness are within acceptable limits to allow direct comparison of structural and electrical properties.

Variation in electrical properties of the Mn_3CuN films grown at deposition pressures of 0.2, 0.3 and 0.5 Pa are shown in Figure 2. The sheet resistance (R_s) (Fig 2a) of the as-grown films is observed to increase with increasing pressure. Films deposited at 0.2 Pa record the lowest average as-grown sheet resistance of 17.7 Ω/□, which increases to 18.5 Ω/□ when deposited at 0.3 Pa, while films deposited at 0.5 Pa show the highest as-grown sheet resistance of 27.3 Ω/□. This increase in sheet resistance is associated with the formation of open-void structures in the thin film textures due to decrease in the energy of ad-atom species at higher deposition pressures [29]. After the first heat treatment stage in N_2 for 3 hours at 325°C, a reduction in sheet resistance is observed for the films deposited at lower deposition pressures of 0.2 and 0.3 Pa to 16.4 Ω/□ and 17.5 Ω/□, respectively. On the other hand, for films deposited at a higher working pressure of 0.5 Pa, sheet resistance increases slightly to 27.4 Ω/□ and the error bars become wider due to oxidation of its more open-void structure. Post-deposition annealing is known to cause densification, defect healing and crystallization in as-grown films [30]. These changes results in better inter-grain conductivity and lead to a reduction in sheet resistance. Stabilization treatment of thin films in air for 16 hours at 260°C, increases sheet resistance of all the samples with a slight increase in the associated error bars, indicative of oxidation of the surface. The final sheet resistance values for the three samples are 21.8, 22.2, and 34.2 Ω/□ for films deposited at 0.2, 0.3 and 0.5 Pa, respectively.

The result for as-grown TCR (Fig 2b) is observed to become more negative with increasing deposition pressure. The films deposited at 0.2 Pa register an average TCR of -335 ppm/ºC, with films deposited at 0.3 Pa registering a slightly more negative value of -340 ppm/ºC, which reduces further -378 ppm/ºC for films deposited at 0.5 Pa. Voids in the as grown films are represented by increased barrier height, which confines charge carriers within grains and thereby increases the resistance of the films [31]. In metals, increasing temperature increases particle collisions, thereby increasing the resistance and thus resulting in a positive TCR. But in intermetallic thin films, increasing temperature can cause increased transport of charge carriers via tunneling or hopping between the grains, thus making the TCR more negative. After each stage of heat treatment, the TCR is observed to shift in a positive direction for all Mn_3CuN films arising from densification, defect healing and crystallization of the films. In addition, this changes the charge carrier transport from grain hopping/tunnelling to carrier collision and thus leads to the emergence of a positive TCR in these films. The films deposited at 0.2 Pa register an average TCR value of -6 ppm/°C after the stabilization treatment stage in air for 16 hours at 260°C. The shifts into the positive TCR region become more pronounced with increasing deposition pressure. The films deposited at 0.3 Pa register a final average TCR value of +15 ppm/°C while films deposited at 0.5 Pa have a higher average value of +37 ppm/°C. Inokuma *at al.* (1985) experimented with adding oxides of various transition metals to control the TCR value of printed resistors and observed that oxides shift the TCR in the negative direction [32]. However, they also observed that addition of Cu oxides shifted the TCR in the positive direction. The open-void nature of the Mn_3CuN films deposited at higher deposition pressure of 0.5Pa, exposes a relatively larger surface area of film to oxidation during the heat treatment stages, thereby increasing the content of Cu oxide within the film. This in turn aids the shift of TCR in the positive direction compared to those at lower deposition pressures of 0.2 and 0.3 Pa. The TCR value of -6 ppm/°C achieved for Mn_3CuN thin films deposited at 0.2 Pa is significantly lower than the values of 46 ppm/°C and 22 ppm/°C reported by Chi *et al.* [6] and Ding *et al*. [5] for the bulk Mn_3CuN and $Mn_3Ni_{0.7}Cu_{0.3}N$ material systems, and similar to the ultra-low TCR value of <6 ppm/°C achieved by Takenaka *et al*. [21] for the $Mn_3Ag_{1-X}Cu_XN$ system in bulk format.

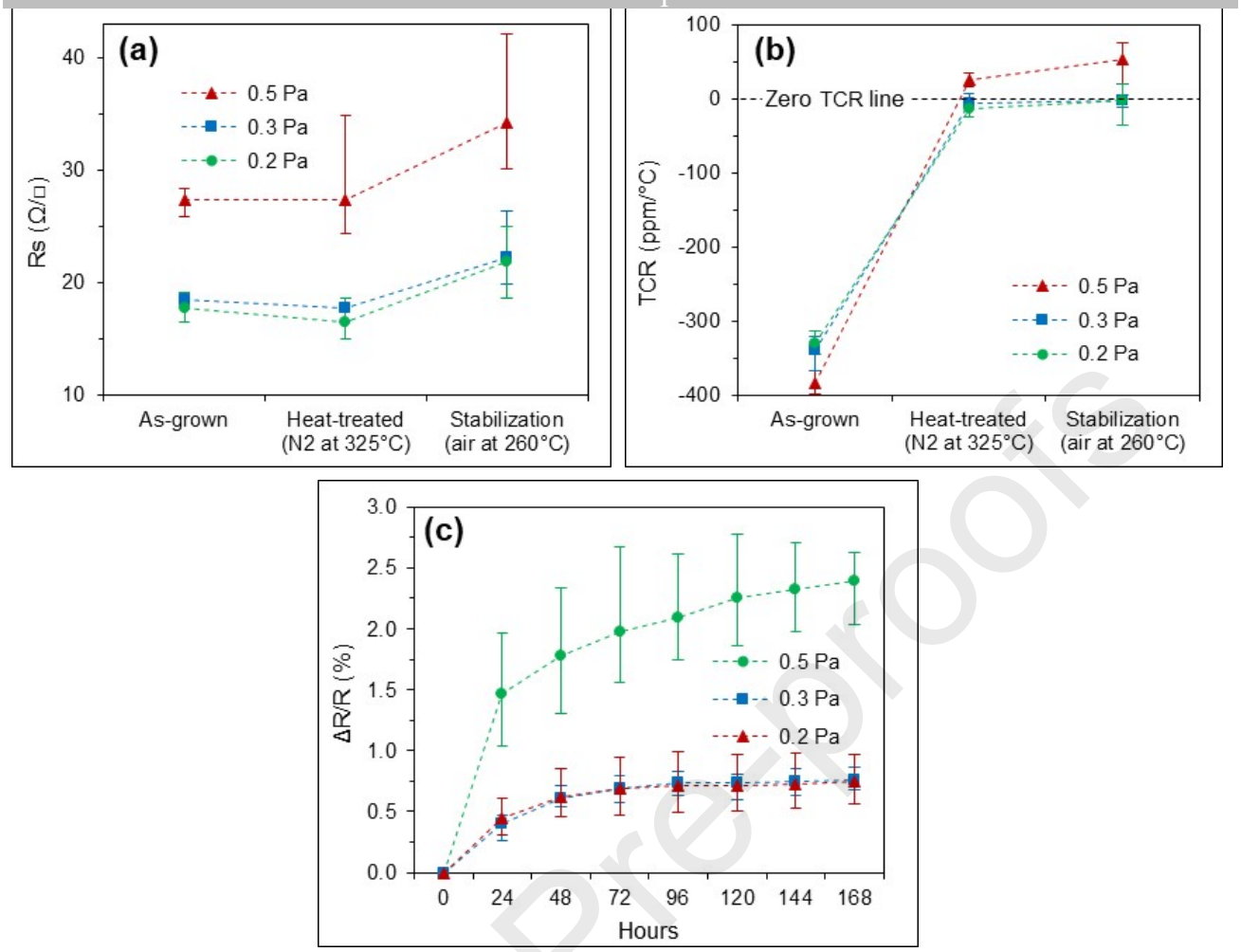

***Figure 2**: Variation in electrical properties of Mn_3CuN films grown at deposition pressures of 0.2, 0.3 and 0.5 Pa. (a) Sheet resistance (Rs) measured at room temperature, and (b) temperature coefficient of resistance (TCR) measured between 20°C and 70°C, as-grown, after heat treatment in N_2 for 3 hours at 325°C, and after stabilization treatment in air for 16 hours at 260°C. (c) Resistance change of pre-stabilized films (ΔR/R) during 1 week (168 hours) of storage in air at 155°C, measured at 155°C.*

Figure 2(c) shows the resistance stability figures achieved for the three samples of Mn_3CuN films grown at different deposition pressures after the dry heat stability test for 1 week (168 hours) at 155°C in air. The stability figure for the films deposited at the highest deposition pressure of 0.5 Pa is observed to be inferior to the films grown at lower deposition pressures of 0.2 and 0.3 Pa. The films deposited at 0.5 Pa had change in resistance values from 2.03% to 2.62%, with an average value of 2.38% after the 168-hour test. However, for the same test, the films deposited at lower pressures of 0.2 Pa and 0.3 Pa registered much lower average resistance changes of 0.74% and 0.76% respectively, with values in the range of 0.57% to 0.97%. This trend is thought to be a result of the open-void structure of the films deposited at higher pressure, making them more susceptible to impurity inclusion and a higher degree of oxidation during the test at higher temperature in air. The reported stability values of <1% are very promising for unprotected resistive thin films [33] and can be improved further by adding protective resin coatings like those used to encapsulate precision thin film resistor components [34].

Figure 3(a) shows the XRD spectra for Mn_3CuN films as-grown at the three varying deposition pressures of 0.2, 0.3 and 0.5 Pa. In contrast to a deposition pressure of 0.5 Pa, which showed an

amorphous film, the films grown at lower deposition pressures of 0.3 and 0.2 Pa show a higher degree of crystallinity with peaks at 46.6º, showing preferential crystal orientation along the (200) plane of the Mn_3CuN antiperovskite structure (ICSD card number 628356). Therefore, the results show that the crystallinity improves as the deposition pressure is reduced. No additional peaks were observed for any of the as-grown films in the full 2θ range of 20° to 90°. This decrease in XRD peak intensity seen for the films deposited at higher deposition pressure aligns well with the corresponding increase in the sheet resistance (Fig 2a). Discontinuities in thin film features responsible for increasing the sheet resistance are also known to decrease the intensity of the crystalline peaks during XRD analysis [35]. Eufinger *et al*. (2006) observed a 5 to 25% reduction in film density of sputter deposited TiO_2 thin films, as deposition pressure was increased from 0.5 to 2.5 Pa, which in their case led to a considerable change in photocatalytic activity of the film [30]. With increase in working pressure, the sputtered particles experience more scattering on their journey towards the substrate, which results in reduced energy when they reach the growing film at the substrate. This phenomenon leads to a reduction in crystallinity, density and a net increase in the open-void nature of the film [36], which in our case, hinders the transport of charge carriers and thereby increases the electrical resistance of the growing film.

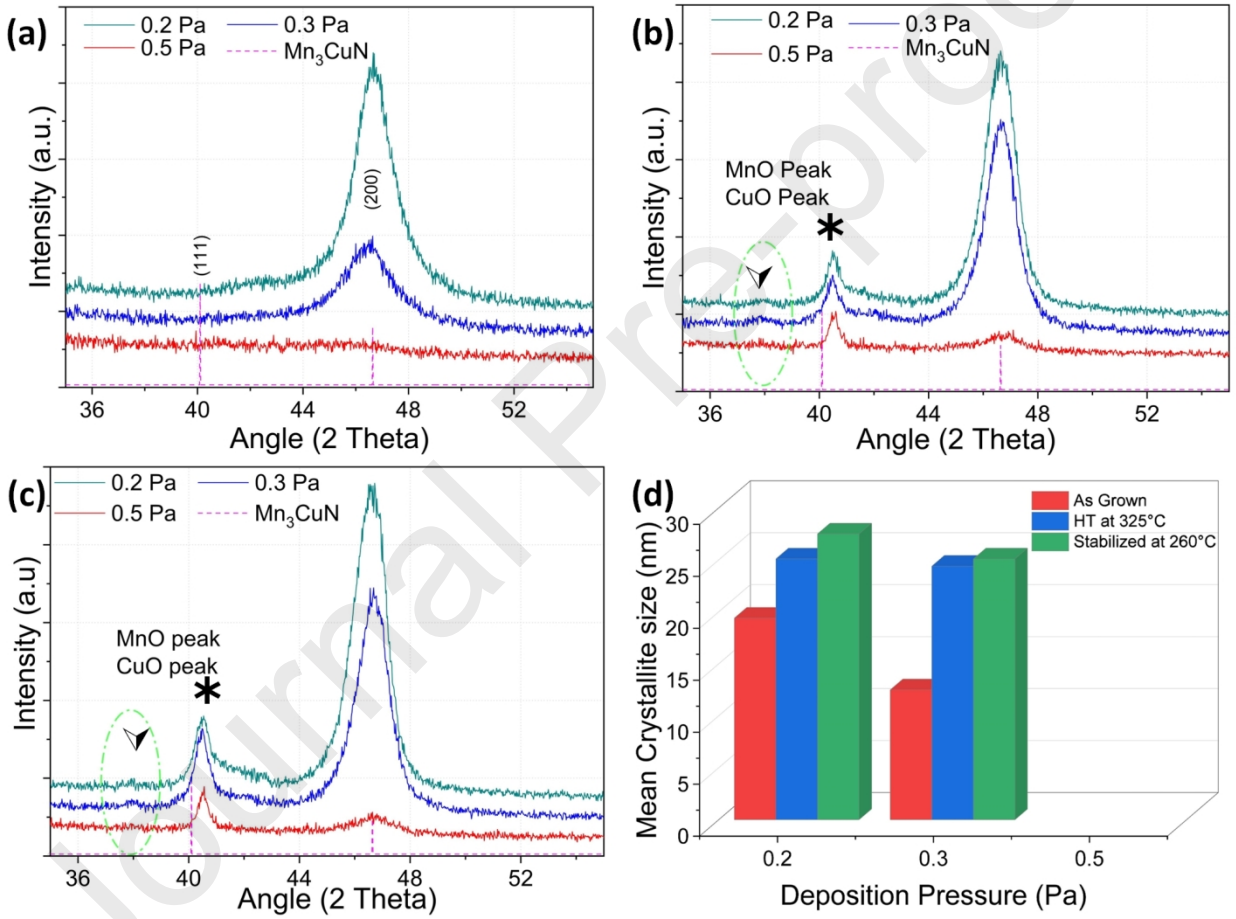

***Figure 3**: XRD spectrums of Mn_3CuN films grown at varying deposition pressures of 0.2, 0.3 and 0.5 Pa. (a) As-grown, (b) After heat treatment in N_2 for 3 hours at 325°C, (c) after stabilization treatment in air for 16 hours at 260°C, and (d) FWHM as and calculated mean crystallite sizes.*

Figure 3(b) shows the XRD spectrum for the three samples of Mn_3CuN films after heat treatment in N_2 for 3 hours at 325°C. For films deposited at the highest pressure of 0.5 Pa, a small protrusion can be observed around the (200) peak of the Mn_3CuN antiperovskite structure, indicating the start of amorphous to crystalline transformation. Heat treatment of these samples results in grain growth, orientation alignment and densification of the film (see Figs 4, 5 and 6), leading to crystallization. However, the energy supplied from the heat treatment is not sufficient to complete the crystallization

process and therefore results in weaker peak intensity. For films grown at lower deposition pressures of 0.2 and 0.3 Pa, the as-grown films are crystalline, and the heat treatment further increases the sharpness of the (200) peak. This result is supported by the decrease in FWHM and corresponding increase in mean crystallite size, calculated from the (200) peak of the Mn_3CuN films grown at 0.2 and 0.3 Pa after heat treatment in N_2 (Fig 3d) (the (200) peak of the film grown at 0.5 Pa was not intense enough to calculate the crystallite size). Films deposited at 0.2 and 0.3 Pa have average calculated crystallite sizes of 19.4 and 12.5 nm in the as-grown state, which increase to values of 25.1 and 24.4 nm, respectively following heat treatment in N_2. This increase in crystallinity of the films is coupled with the emergence of peaks around 40.8°, characteristic of manganese oxide (MnO) [37]. The appearance and intensity of this MnO peak remains comparable for all the films irrespective of deposition pressure. There is also a weak reflection around 38.4°, indicative of the (111) phase of tenorite copper oxide (CuO), which is expected for heat treatment temperatures above 300°C [38, 39]. Crystallization and defect healing aid a reduction in sheet resistance, while open-void structure and oxide formation increase sheet resistance, and therefore, the limited change in sheet resistance values seen after the first stage of heat treatment (Fig 2a) is a result of these competing effects cancelling each other out.

The crystal structures of the three Mn_3CuN film samples after stabilization treatment in air for 16 hours at 260°C are shown in Figure 3(c). It can be again observed that the (200) peak at around 46.6°, representing the antiperovskite structure, sharpens further for the films grown at 0.2 and 0.3 Pa, with a corresponding small increment in average crystallite sizes to 27.5 and 25.1 nm, respectively. The MnO peak at 40.8° also grows in intensity, indicating more oxidation of the films when exposed to open air at high stabilizing temperature of 260°C. No other peaks are observed, which indicates that there is no degradation of the existing structure, and therefore, it is reasonable to suggest that all three films maintain a stable Mn_3CuN antiperovskite structure at heat treatment temperatures up to 325°C in N_2 and 260°C in air.

The change in the surface topology and corresponding surface roughness of the Mn_3CuN films deposited at different pressures, as grown and following heat treatment in N_2 and stabilization in air can be seen in the AFM images in Figure 4. In the as-grown state, the films deposited at 0.2 and 0.3 Pa are smoother (mean surface roughness R_a<0.9 nm). The film deposited at 0.5 Pa has a mean surface roughness value >2.9 nm, which is three times larger than those deposited at 0.2 and 0.3 Pa. Heat treatment in N_2 leads to formation of a rough layer on the surface of the films, which is known to be MnO, observed as a peak around 40.8° in the XRD spectrums (Fig 3). After the first stage of heat treatment, the surface topology looks almost identical for all film specimens regardless of deposition pressure. The measured surface roughness values are also very similar (7.27 to 8.69 nm). However, after stabilization treatment in air the trend in topography becomes similar to that of the as-grown films, with the films deposited at 0.2 and 0.3 Pa having a more densely packed and smoother surface (5.88 to 6.02 nm mean roughness) than the films deposited at 0.5 Pa (10.41 nm mean roughness).

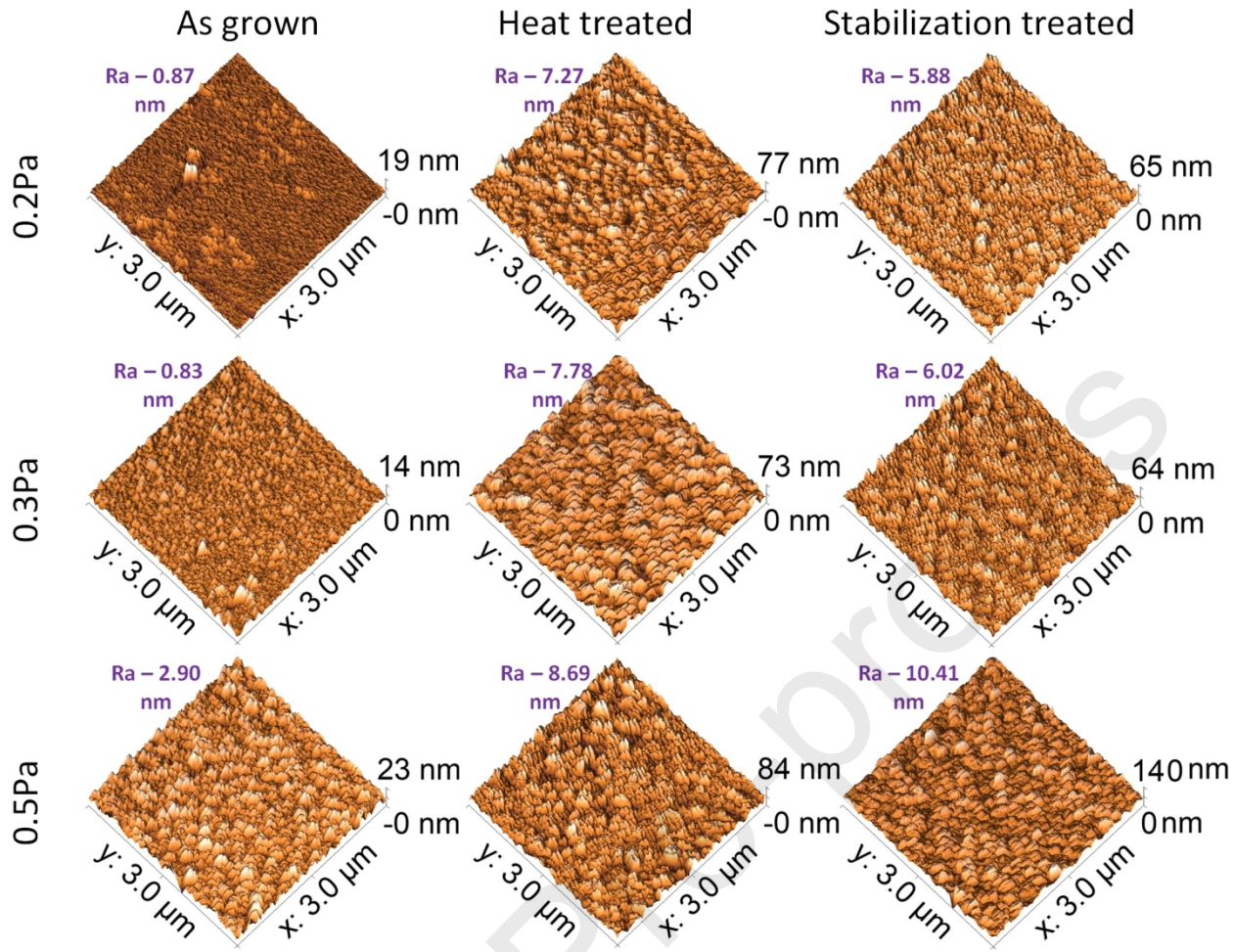

***Figure 4**: AFM images of Mn_3CuN films grown at varying deposition pressures of 0.2, 0.3 and 0.5 Pa, As-grown, after heat treatment in N_2 for 3 hours at 325°C, and after stabilization treatment in air for 16 hours at 260°C.*

Further, SEM imaging was performed to study the changes in the surface morphology of the deposited thin films after each process stage, see Figure 5. The as-grown film deposited at 0.5 Pa has well defined oval structures of varying sizes but as the deposition pressure is reduced, the features reduce in number. For the film deposited at 0.3 Pa, there are very few circular structures dispersed on the surface, and they become almost nonexistent for the film grown at 0.2 Pa. After heat treatment, visible dendrite like features develop on the surface of the films, making the surface appearance rougher. Other studies have shown Mn rich thin films developing such dendrite like features of MnO during thermal processing, due to migration of Mn to the surface [40, 41]. Because of its low thermodynamic oxidation potential ($\Delta G(Cu_2O) = -146.2$; $\Delta G(CuO) = -127.1$; $\Delta G(MnO) = -362.8$ kJ/mol), the probability of formation of MnO is higher than that of CuO [42]. Among the three samples, the film grown at 0.2 Pa shows the largest concentration of these dendrites and this aligns well with increased surface roughness observed for this sample (Fig 4). After stabilization heat treatment in air, formation of these dendrites subsides and is overtaken by growth of surrounding surface features. These results show that after the first stage of heat treatment, the Mn migrates to the surface and forms the dendrite like features of MnO but during stabilization heat treatment, Cu also takes part in this oxidation process which leads to growth of additional surface features, thus completing the self-passivation of the surface layers. It is the completion of this self-passivation process of the upper layer that improves the resistance stability of thin film layer.

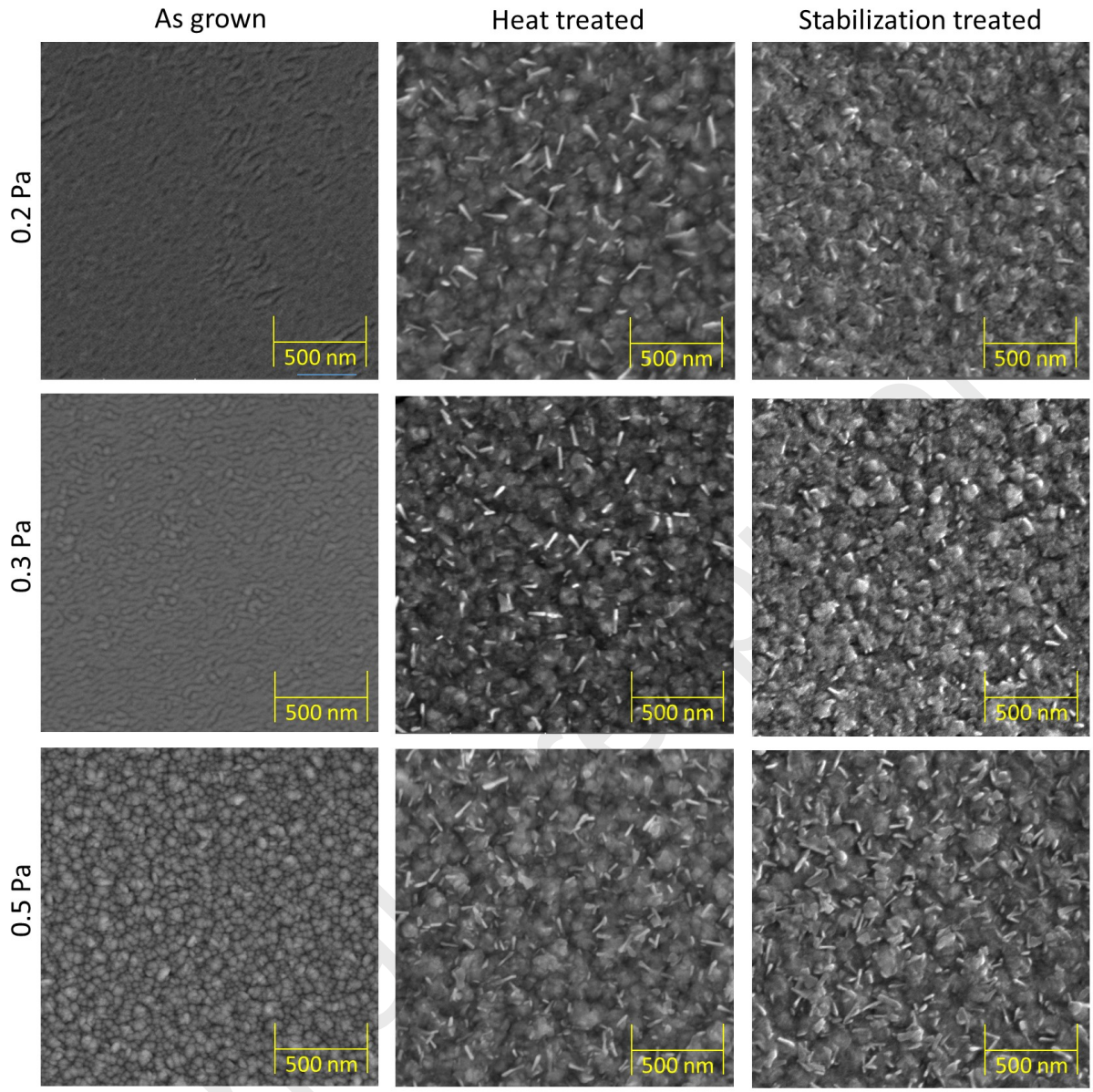

***Figure 5**: SEM surface images of Mn_3CuN films grown at varying deposition pressures of 0.2, 0.3 and 0.5 Pa, as-grown, after heat treatment in N_2 for 3 hours at 325°C, and after stabilization treatment in air for 16 hours at 260°C.*

The cross sections of the deposited thin films were also analyzed by SEM after each process stage to observe their effect on the antiperovskite layer, see Figure 6. The as-grown thin films have thicknesses in the range of 434 to 483 nm, which is in good agreement with the values measured using the profilometer (Fig 1e). The films deposited at a higher pressure of 0.5 Pa were thicker in comparison to those deposited at lower deposition pressures. The films deposited at the lowest deposition pressure of 0.2 Pa show tightly packed tapered columns and with increase in pressure to 0.3 and 0.5 Pa these columns begin to separate. This further supports the increased density at lower deposition pressures. However, after the first stage of heat treatment, the overall thickness (D1) of the film increases together with a newly formed upper layer (D2) on the surface of all three films. This new layer is formed by the oxidation of the surface [43, 44]and its thickness remains around 120 nm. There is also a slight increase in the thickness range of the lower Mn_3CuN layer. Following the second stage of air stabilization treatment, all three films have similar Mn_3CuN layer thicknesses

(~ 510 nm) irrespective of deposition pressure. The thickness of the upper MnO layer is also comparable for all three films. The film deposited at the lowest deposition pressure of 0.2 Pa has a very densely packed structure with almost undistinguishable columns, whereas for the film deposited at 0.3 Pa the column boundaries are more apparent. The film deposited at 0.5 Pa shows a very different structure consisting of more random shaped grains with frequent spaces between them. This more amorphous and less dense nature is in good agreement with the XRD spectra in Figure 3. Overall, the thickness increase can be explained semi quantitatively by the phase change from Mn_3CuN to MnO (or MnO-CuO mixture). Although the thickness change of the 0.5 Pa sample is smaller from as-grown to after heat treatment, it can be explained by a combination of the densification and oxidation of the lower Mn_3CuN layer during heat treatment.

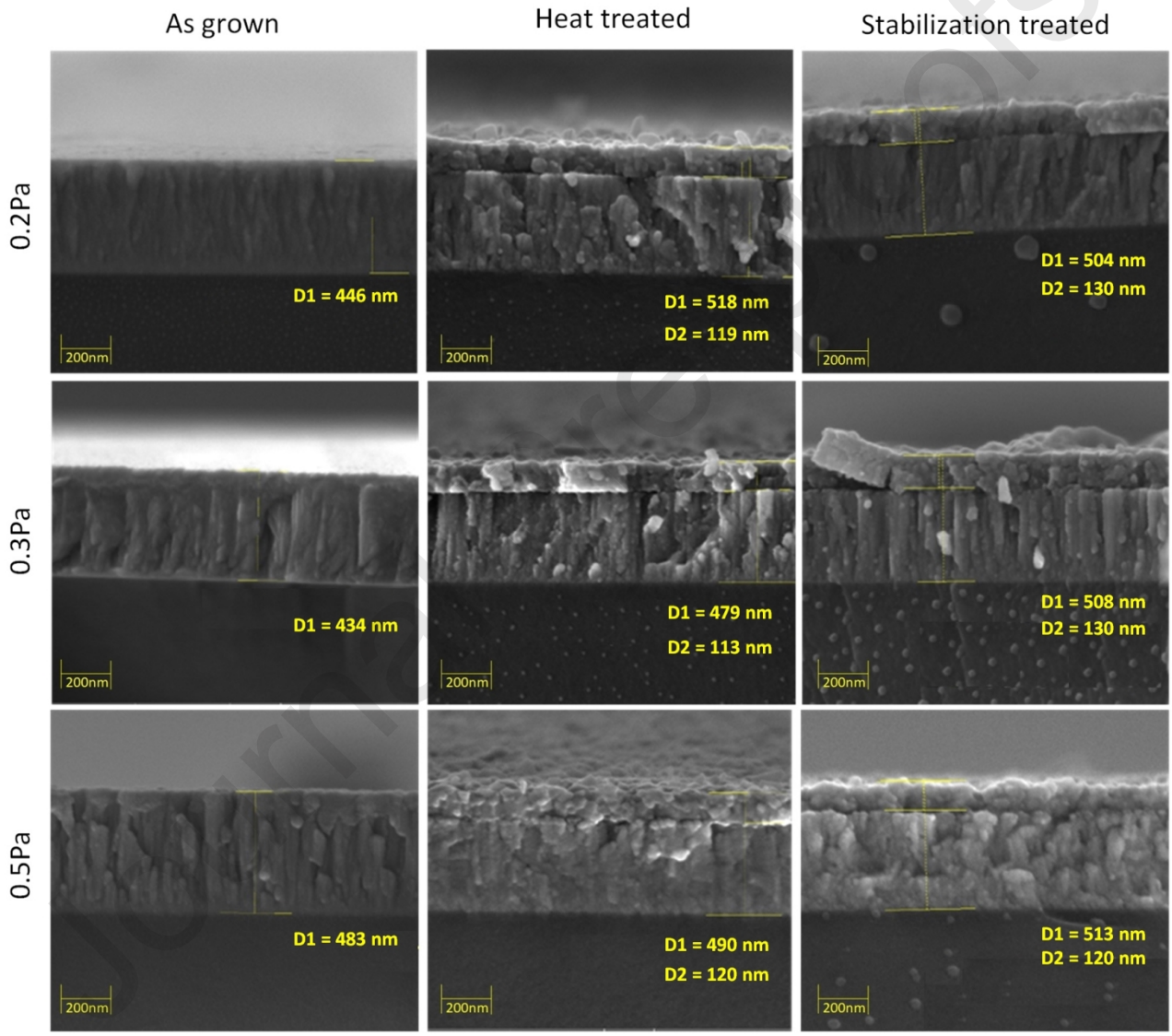

Figure 6: *SEM cross sectional images of Mn_3CuN films grown at varying deposition pressures of 0.2, 0.3 and 0.5 Pa, as-grown, after heat treatment in N_2 for 3 hours at 325°C, and after stabilization treatment in air for 16 hours at 260°C.*

Figure 7 shows the results of low-voltage (5 KeV) EDX chemical analysis carried out on the cross sections of the films grown at varying deposition pressure. Two sites were measured on the lower

Mn_3CuN antiperovskite layer, while one site was measured on the upper MnO layer of each film. An additional site on the underlying glass substrate was measured to provide a reference. At this site, Si and O_2 were the main constituents, roughly in 2:1 atomic ratio, indicating SiO_2 along with traces of Na, Ca, and Mg, as expected in soda lime glass. The results also show a very clear correlation between the content of Cu in the upper layer and the deposition pressure. For the film deposited at 0.2 Pa, no Cu is observed in the upper layer, which increases to 1.2 at.% Cu for the film deposited at 0.3 Pa. This figure then increases abruptly to a value of 20.7 at.% Cu for the film deposited at 0.5 Pa. Similar to Inokuma *at al.* who observed that addition of Cu oxides shifted the TCR of printed resistors in the positive direction, Valladares *et al.* also reported that grains of CuO crystallizing around 300°C, pushes the TCR in the positive direction, whereas the oxides of manganese produce a shift in the negative direction [32, 45]. This result correlates well with the observation of CuO in the XRD spectra (Fig 3) and strengthens the previous suggestion that the presence CuO is responsible for shifting the TCR value of the film deposited at 0.5 Pa in positive direction during heat treatment (Fig 2b), while also leading to inferior resistance stability (Fig 2c). The steep increase in the Cu concentration in the upper layer for samples deposited at 0.5 Pa could be explained as a combination of the reduction in the film density and the depletion of Mn on the surface for oxidation. Work done by Oleshkevych *et al.* shows that the oxygen affinity of Mn will drive the transport of Mn to the surface even in low O_2 environments and in this case it will lead to the dealloying of the underlying antiperovskite layer [46, 47]. This release of free Cu in the matrix will lead to the diffusion of the Cu to the upper surface and this diffusion becomes exaggerated for films with reduced density, like those grown at 0.5 Pa in this work [46, 48, 49]. With the reducing density at higher deposition pressure, the protection provided by the upper layer also appears to be less effective, as a much higher O content of 25.0 at.% is found in the lower Mn_3CuN layer of the film deposited at 0.5 Pa, when compared to the values of 4.1 and 8.3 at.% seen in the films deposited at 0.2 and 0.3 Pa, respectively. This result further supports the proposition that depositing the Mn_3CuN antiperovskite structure at lower pressure is more beneficial to produce films with higher density and increased protection from the surrounding environment that offer enhanced TCR and resistance stability performance.

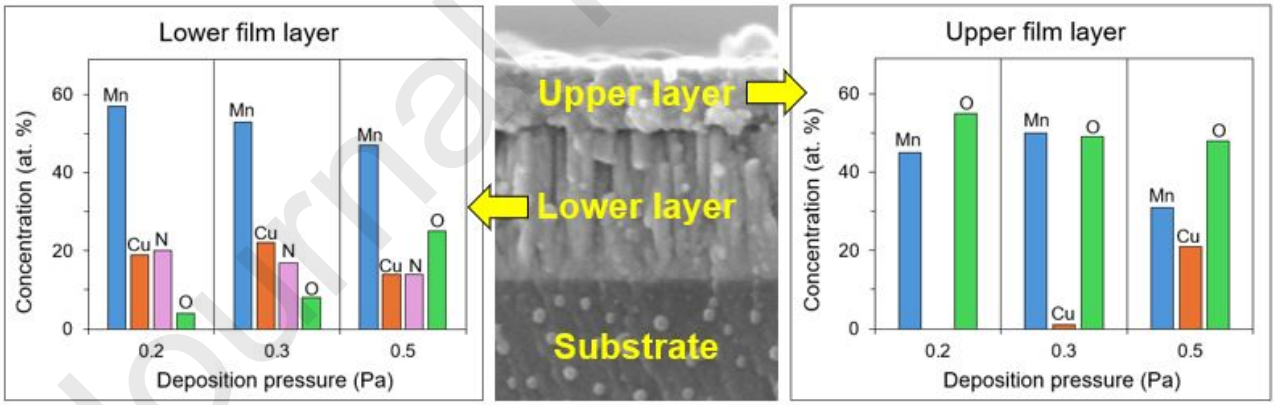

Figure 7: *Chemical composition of the upper and lower layers of Mn_3CuN films deposited at varying pressure, after stabilization treatment in air for 16 hours at 260°.*

4. Conclusion

In this study, deposition pressure is shown to have a pronounced effect on the morphological features, chemical composition, and electrical properties of Mn_3CuN antiperovskite thin film

structures. Mn_3CuN films deposited at a higher deposition pressure of 0.5 Pa are observed to have an open-void structure, which leads to an increase in their sheet resistance, and inferior TCR and resistance stability when compared to films deposited at lower deposition pressures of 0.2 and 0.3 Pa. Films deposited at the lowest deposition pressure of 0.2 Pa showed a much denser and stable structure with sheet resistance values of ~20 Ω/□, an extremely low TCR value of -6 ppm/°C after stabilization treatment for 16 hours in air at 260°C and improved resistance stability down to 0.57% for unprotected films, following storage for 168 hours in air at 155°C. It is therefore recommended that the fabrication of Mn_3CuN antiperovskite thin films be carried at lower deposition pressure for the future development of high precision thin film resistive components.

Acknowledgements

This work was supported by a collaborative partnership between Northumbria University and TT Electronics PLC, Bedlington, UK. TT Electronics PLC supplied the prescribed alumina substrates with silver conductor pads used in this experiment. IRC TT, Corpus Christi, USA, a subsidiary of TT Electronics PLC, shared insight into key production stages of extremely low TCR passive components.

Data availability

Data will be made available on request.

References

1. Chu, L.-H., et al., *Doping effect of Co at Ag sites in antiperovskite Mn3AgN compounds.* Chinese Phys Lett, 2015. **32**(4): p. 047501.

2. E.O.Chi, W.S.Kim, and N.H.Hur, *nearly zero temperature coefficient of resistiivty in antiperovskite compound CuNMn3.* Solid state communication 2001. **120**: p. 307-310.

3. Ying, S., et al., *The unusual resistivity behavior and correlated magnetic properties of antiperovskite Mn3Ag[1−x]M[x]N (M = Sn, Zn) compounds.* Sci Adv Mater, 2014. **6**(7): p. 1394-1398.

4. Sun, Y., et al., *Low temperature coefficient of resistivity induced by magnetic transition and lattice contraction in Mn3NiN compound.* Scripta Materialia, 2010. **62**(9): p. 686-689.

5. Lei, D., et al., *Near zero temperature coefficient of resistivity in antiperovskite Mn3Ni1−xCuxN.* Applied Physics Letters, 2011. **99**(25): p. 251905.

6. E.O. Chi, W.S.K., N.H. Hur, *Nearly zero temperature coefficient of resistivity in antiperovskite compound CuNMn3.* Solid State Communications, 2001. **120**(7-8): p. 307-310.

7. Lukose, C.C., G. Zoppi, and M. Birkett, *Thin film resistive materials: past, present and future.* IOP Conf. Ser.: Mater. Sci. Eng., 2016. **104**: p. 012003.

8. Lin, C.-H., et al., *A study on the NiCrMnZr thin film resistors prepared using the magnetron sputtering technique.* Thin Solid Films, 2018.

9. Yin, Y., et al., *Critical behavior in the antiperovskite Mn3CuN at ferromagnetic to paramagnetic phase transition.* Journal of Magnetism and Magnetic Materials, 2013. **346**: p. 203-208.

10. Shibayama, T. and K. Takenaka, *Giant magnetostriction in antiperovskite Mn3CuN.* Journal of Applied Physics, 2011. **109**(7): p. 07A928.

11. Ming-Hui, Y., L.H. Lewis, and A.R. Moodenbaugh, *Large magnetic entropy change in the metallic antiperovskite Mn3GaC.* Journal of Applied Physics, 2003. **93**(12): p. 10128.

12. Na, Y., et al., *Structure and properties of ternary manganese nitride Mn3CuNy thin films fabricated by facing target magnetron sputtering.* Materials Research Bulletin, 2011. **46**(7): p. 1022-1027.

13. Lukose, C.C., G. Zoppi, and M. Birkett, *Mn3Ag(1-x)Cu(x)N antiperovskite thin films with ultra-low temperature coefficient of resistance.* J Mater Sci Tech, 2022. **99**: p. 138-147.

14. Khalladi, R., et al., *Magnetic properties study of the anti-perovskite Mn3CuN compound by Monte Carlo simulations.* Solid State Communications, 2019. **290**: p. 42-48.

15. Singh, H.K., et al., *Multifunctional antiperovskites driven by strong magnetostructural coupling.* npj Computational Materials, 2021. **7**(1): p. 98.

16. Çakır, Ö., et al., *Heterogeneous magnetism and kinetic arrest in antiperovskite Mn3-xNixGaC compounds with Ni2MnGa Heusler insertions.* Physical Review B, 2020. **102**(2): p. 024431.

17. Quintela, C.X., et al., *Epitaxial antiperovskite/perovskite heterostructures for materials design.* Science Advances. **6**(30): p. eaba4017.

18. Ying, S., et al., *Investigation of antiperovskite Mn3CuNx film prepared by DC reactive magnetron sputtering.* Materials Research Bulletin, 2010. **45**(9): p. 1230-1233.

19. Fruchart, D. and E. F. Bertaut, *Magnetic studies of the metallic perovskite-type compounds of manganese.* Journal of the Physical Society of Japan, 1978. **44**(3): p. 781-791.

20. Lu, N.P., et al., *Ternary Mn3NMn1−xAgx compound films of nearly constant electrical resistivity and their magnetic transport behaviour.* Journal of Physics D: Applied Physics, 2016. **49**(4): p. 045308.

21. Takenaka, K., et al., *Extremely low temperature coefficient of resistance in antiperovskite Mn3Ag1−xCuxN.* Applied Physics Letters, 2011. **98**(2): p. 022103.

22. Oe, T., et al., *Optimization of Mn3Ag1−xCuxN Antiperovskite Compound Fabrication for Resistance Standard.* IEEE TRANSACTIONS ON INSTRUMENTATION AND MEASUREMENT, 2013. **62** (6): p. 4.

23. Masahiro, A., T. Koshi, and I. Hiroshi, *Sputter deposition and characterization of Mn3CuN thin films.* Journal of Alloys and Compounds, 2013. **577**: p. S314-S317.

24. Birkett, M., et al., *Structural and electrical properties of CuAlMo thin films prepared by magnetron sputtering.* Thin Solid Films, 2013. **540**: p. 235-241.

25. Muniz, F.T.L., et al., *The Scherrer equation and the dynamical theory of X-ray diffraction.* Acta Cryst A, 2016. **72**(3): p. 385-390.

26. Vincent, L. and P. Soille, *Watersheds in Digital Spaces: An Efficient Algorithm Based on Immersion Simulations* IEEE Trans Pattern Anal Mach, 1991. **13**(6): p. 583-598.

27. Zheng, W.T., et al., *Reactive magnetron sputter deposited CNx: Effects of N2 pressure and growth temperature on film composition, bonding, and microstructure.* J Vac Sci Technol A: Vac, 1996. **14**(5): p. 2696-2701.

28. Can, W., et al., *Effects of oxygen pressure on lattice parameter, orientation, surface morphology and deposition rate of (Ba0.02Sr0.98)TiO3 thin films grown on MgO substrate by pulsed laser deposition.* Thin Solid Films, 2005. **485**(1): p. 82-89.

29. Kusano, E., *Structure-Zone Modeling of Sputter-Deposited Thin Films: A Brief Review.* Appl Sci Converg Technol, 2019. **28**(6): p. 179-185.

30. Eufinger, K., et al., *Effect of microstructure and crystallinity on the photocatalytic activity of TiO2 thin films deposited by dc magnetron sputtering.* Journal of Physics D: Applied Physics, 2007. **40**(17): p. 5232-5238.

31. Arun, P. and A.G. Vedeshwar, *Influence of grain size on the electrical properties of Sb2Te3 polycrystalline films.* Materials Research Bulletin, 2003. **38**(15): p. 1929-1938.

32. TAKETA, T.I.Y., *Control of Electrical Properties of RuO2 Thick Film Resistors.* Act Passive Electron Compon, 1985. **12**: p. 155-66.

33. Wang, X.Y., et al., *Deposition of Cr–Si–Ni–Mo films at a low sputtering current and performance of heat and humid resistance.* Applied Surface Science, 2014. **289**: p. 538-544.

34. Hahtela, O., et al., *Atomic layer deposited alumina (Al2O3) coating on thin film cryoresistors*, in *2008 Conference on Precision Electromagnetic Measurements Digest*. 2008. p. 272-273.

35. Salunkhe, R.R., et al., *Chemical synthesis and electrochemical analysis of nickel cobaltite nanostructures for supercapacitor applications.* Journal of Alloys and Compounds, 2011. **509**(23): p. 6677-6682.

36. Mahieu, S., et al., *Biaxial alignment in sputter deposited thin films.* THIN SOLID FILMS, 2006. **515**(4): p. 1229-1249.

37. Kim, J.-H., et al., *Electrical Properties of Zn(Mn,Co)O Films Grown by Pulsed Laser Deposition Method.* ECS Transactions, 2008. **16**(12): p. 27-31.

38. Ali, S.G., et al., *Green Synthesis of Copper Oxide Nanoparticles from the Leaves of Aegle marmelos and Their Antimicrobial Activity and Photocatalytic Activities.* Molecules, 2023. **28**(22).

39. Raship, N.A., et al., *Effect of annealing temperature on the properties of copper oxide films prepared by dip coating technique.* AIP Conf Proc, 2017. **1788**: p. 030121.

40. Anukaliani, A. and M. Nirmala, *Structural and optical properties of an undoped and Mn doped ZnO nanocrysatlline thin film.* Photonics Letters of Poland, 2010. **2**(4).

41. Mondal, S., S.R. Bhattacharyya, and P. Mitra, *Preparation of manganese-doped ZnO thin films and their characterization.* Bulletin of Materials Science, 2013. **36**(2): p. 223-229.

42. Bakieva, O.R., et al., *Composition, structure, and corrosion electrochemical properties of copper–manganese alloy subjected to argon ion implantation.* Phys Met Metallogr, 2020. **121**(1): p. 46-52.

43. De Los Santos Valladares, L., et al., *Characterization of Ni thin films following thermal oxidation in air.* J Vac Sci Technol B, 2014. **32**(5): p. 051808.

44. Yang, S., et al., *Tuning structural colors of TiO2 thin films using an electrochemical process.* Molecules, 2022. **27**(15): p. 4932.

45. De Los Santos Valladares, L., et al., *Crystallization and electrical resistivity of Cu2O and CuO obtained by thermal oxidation of Cu thin films on SiO2/Si substrates.* Thin Solid Films, 2012. **520**(20): p. 6368-6374.

46. Oleshkevych, A.I., et al., *Enhanced diffusion caused by surface reactions in thin films of Sn–Cu–Mn.* Thin Solid Films, 2014. **550**: p. 723-731.

47. Hengge, E., et al., *Porosity evolution and oxide formation in bulk nanoporous copper dealloyed from a copper-manganese alloy studied by in situ resistometry.* Nanoscale Adv, 2023. **5**(2): p. 393-404.

48. Su, Y.-S., et al., *A study on the diffuse mechanism and the barrier property of copper manganese alloy on tantalum.* IEEE J Electron Devices Soc, 2015. **3**(3): p. 284-290.

49. Lee, W.-H., et al., *Effect of density on the diffusion barrier property of TiNx films between Cu and Si.* Mater Chem Phys, 2004. **85**(2-3): p. 444-449.

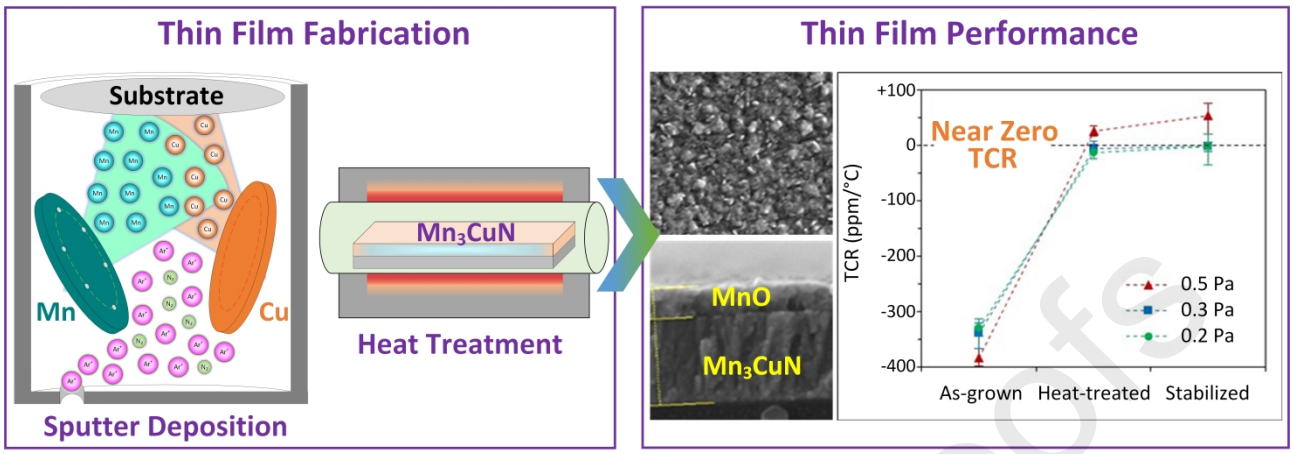

Highlights

- Growth of Mn_3CuN thin films with near-zero temperature coefficient of resistance (TCR).
- Decreasing deposition pressure improves film density and resistance stability.
- Heat treatment forms protective MnO layer to fine tune electrical properties.
- Mn_3CuN films grown at 0.2 Pa have TCR <6 ppm/°C and resistance stability <0.6%.

Declaration of interests

☒ The authors declare that they have no known competing financial interests or personal relationships that could have appeared to influence the work reported in this paper.

☐ The authors declare the following financial interests/personal relationships which may be considered as potential competing interests: